Effect of Surfactants' Tail Number on the PVDF/GO/TiO$_2$-Based Nanofiltration Membrane for Dye Rejection and Antifouling Performance Improvement

R. Mohamat, A. B. Suriani, A. Mohamed, Muqoyyanah, M. H. D. Othman, R. Rohani, M. H. Mamat, M. K. Ahmad, M. N. Azlan, M. A. Mohamed, et al.

ONLINE FIRST

Springer

Springer

RESEARCH PAPER

Effect of Surfactants' Tail Number on the PVDF/GO/TiO$_2$-Based Nanofiltration Membrane for Dye Rejection and Antifouling Performance Improvement

R. Mohamat[1,2] · A. B. Suriani[1,2] · A. Mohamed[1,3] · Muqoyyanah[1,2] · M. H. D. Othman[4] · R. Rohani[5] · M. H. Mamat[6] · M. K. Ahmad[7] · M. N. Azlan[2] · M. A. Mohamed[8] · M. D. Birowosuto[9] · T. Soga[10]

Abstract

In this work, the novel utilisation of customised double- and triple-tail sodium *bis*(3,5,5-trimethyl-1-hexyl) sulphosuccinate (AOT4) and sodium 1,4-*bis*(neopentyloxy)-3-(neopentyloxycarbonyl)-1,4-dioxobutane-2-silphonate (TC14) surfactants to assist the direct graphene oxide (GO) synthesis via electrochemical exfoliation utilising dimethylacetamide (DMAc) as a solvent were investigated. The synthesised DMAc-based GO and titanium dioxide (TiO$_2$) nanoparticles were then used to fabricate polyvinylidene fluoride (PVDF)-based nanofiltration (NF) membranes by the non-solvent-induced phase separation method. The incorporation of GO and TiO$_2$ as hydrophilic nanoparticles were to enhance membrane hydrophilicity. The utilisation of higher surfactants' tail number obviously alters the fabricated membrane's morphology which further affects its performance for dye rejection and antifouling ability. Higher surfactants' tail number resulted in higher oxidation process which then provided more interaction between the GO and PVDF. Based on the dead-end cell measurement, PVDF/TC14-GO/TiO$_2$ presented a slightly higher dye rejection efficiency of 92.61% as compared to PVDF/AOT4-GO/TiO$_2$ membrane (92.39%). However, PVDF/TC14-GO/TiO$_2$ possessed three times higher water permeability (48.968 L/m^2 h MPa) than PVDF/AOT4-GO/TiO$_2$ (16.533 L/m^2 h MPa) and also higher hydrophilicity as presented by lower contact angle (65.4 ± 0.17°). This confirmed that higher surfactants' tail number improved the fabricated membrane's performance. Both fabricated membranes also exhibited high flux recovery ratio (FRR) (> 100%) which indicated better antifouling properties.

Graphic abstract
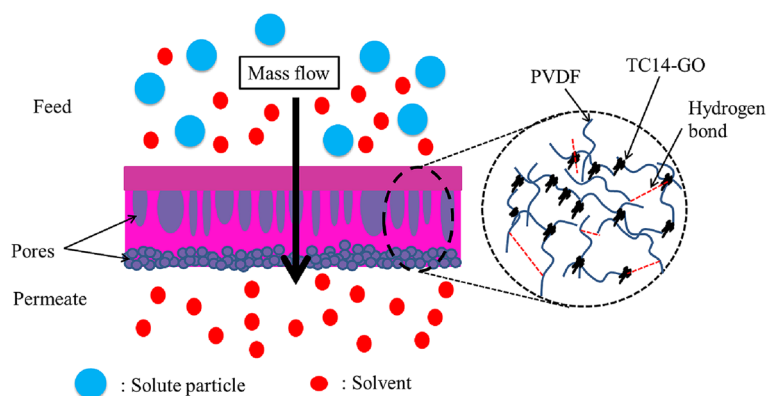
✉ A. B. Suriani
  absuriani@yahoo.com

Extended author information available on the last page of the article

Article Highlights

- **High dye rejection by using simpler electrochemical exfoliation utilising surfactant for GO synthesis.**
- **Improved water permeability by utilising triple-tail-based GO.**
- **Enhanced hydrophilicity by utilising triple-tail-based GO.**
- **Higher membrane porosity by utilising triple-tail-based GO.**
- **High antifouling performance by different surfactants' tail number.**

Introduction

The rapid growth of various industries such as paints, textile, printing inks, paper, and plastics causes both high polluted water and high demand for clean water, simultaneously. These industries, especially textile and dyeing industries utilised a large amount of synthetic dyes to colour their product which resulted in large amount of polluted wastewater and released to the environment. Dyes presence can affect water quality since they are toxic and non-biodegradable (Liu et al. 2019; Tran et al. 2019; Yao et al. 2015). Therefore, the removal of this kind of pollutant is crucially needed. Numerous approaches have been attempted to find an effective method to treat polluted water to protect human health and the environment (Santhosh et al. 2016). Among various dye removal methods, membrane separation is one of the versatile and effective technologies to remove polluted water, such as dye contamination (García et al. 2020; Liu et al. 2017). This was due to its several advantages, such as no phase changes, simple in operation, and relatively low energy consumption (Kang and Cao 2014). Over the past few decades, it becomes popular and plays an important role in major industries for water purification, metal recovery and protein separation (Escobar and Van Der Bruggen 2015).

Membrane separation technology has become promising in many type of filtration such as microfiltration, ultrafiltration (UF), nanofiltration (NF), and reverse osmosis (RO). All of these types of filtration are classified based on their membrane properties and separation principle. Recently, the NF membrane has widely applied for water treatment due to its small pore size (1–5 nm) compared to UF, low operating pressure (4–20 MPa) and high water permeability than RO and its capability to retain high valence ions and low molecular weight (Park et al. 2012; Shon et al. 2013). The polymeric membrane can be fabricated by different technique such as sintering, stretching, track-etching and phase inversion (Liao et al. 2018). Among them, the phase inversion method is commonly used due to its several advantages, such as applicable for various polymers, simple in preparation and easy optimisation of membrane thickness and pore size (Ladewig & Al-Shaeli, 2017; Sangermano et al. 2015).

Synthetic polymer membrane namely polyvinylidene fluoride (PVDF), a semicrystalline polymer with repeating units of $-CH_2-CF_2-$, has been extensively used in water treatment processes due to its outstanding physical and chemical properties (Aid et al. 2019; Anvari et al. 2017; Contreras et al. 2018; Kang and Cao 2014; Sangermano et al. 2015). However, the hydrophobic nature of the PVDF membrane causes some critical problems which limit its application due to the membrane fouling during the separation process (Li et al. 2015; Wu et al. 2018). The membrane fouling causes the decline in water flux permeability, shortening membrane lifetime and altering membrane selectivity thus decreased the membrane performance (Teng et al. 2020; Wu et al. 2020; Zhang et al. 2016). Therefore, several approaches have been developed to increase the hydrophilicity properties of PVDF membrane such as physical and chemical modification with hydrophilic organic and inorganic materials (Kang and Cao 2014; Xia and Ni 2014). Among these approaches, a physical modification of blending with organic or inorganic materials has been widely used due to its advantage of facile preparation method through phase inversion. Recently, organic materials-blended PVDF (PMMA, PVAC, PA6) (Freire et al. 2012; Vo and Giannelis 2007), metal oxide particles [aluminium oxide (Al_2O_3), titanium dioxide (TiO_2) and zinc oxide (ZnO)] (Li et al. 2015; Liu et al. 2018), carbon nanotubes (CNTs) (Sivakumaran et al. 2016; Zheng et al. 2009) and graphene oxide (GO) (Wu et al. 2018) have been utilised to enhance the PVDF membrane properties by increasing antifouling effect, permeability and membrane selectivity.

In particular, a potential candidate to effectively reinforce PVDF polymeric materials is TiO_2 due to its excellent properties such as hydrophilicity, chemical stability, low toxicity and commercial availability. TiO_2 is considered the best metal oxide to overcome the fouling issues by increasing the membrane hydrophilicity (Liu et al. 2018; Wu et al. 2018). In addition, it also possesses a small particle size and a large surface area (Park et al. 2018). Several reports have demonstrated that the utilisation of TiO_2 could improve the fouling resistance by increasing the membrane hydrophilicity. Wang et al. (2017) showed that introduction of TiO_2 into the GO-based membrane presents low relative flux reduction (24%)

as compared to pristine GO-based membrane (74%). This low value in relative flux reduction indicates a great anti-fouling property (Wang et al. 2015). The result obtained by Zhang et al. (2017) showed an improvement in antifouling properties when the Ti and O element on the membrane increased as compared to the pristine membrane. This indicated that the hydrophilicity of the membrane was enhanced with the TiO$_2$ present (Zhang et al. 2017). Méricq et al. (2015) also showed the improvement of membrane structure, hydrophilicity properties and permeability when TiO$_2$ nanoparticles were used as an additive for membrane fabrication.

On the other side, GO was also utilised as an additive to fabricate a hydrophilic membrane. GO offers many advantages for water treatment due to its large surface area (calculated up to 2630 m^{2}g^{-1}) (Huang et al. 2012), good chemical stability and high mechanical strength (Young modulus ~ 1 TPa) (Lee et al. 2008). As exfoliated GO contains a considerable number of oxygen-functional groups, such as carboxyl, carbonyl, epoxy, and hydroxyl groups, GO is highly hydrophilic (Miao et al. 2017; Zhang et al. 2013). GO can be synthesised by using a chemical approach, such as Hummers' method and electrochemical exfoliation. The common Hummers' method resulted a high quality of the synthesised GO. However, this method involved high hazardous chemical consumption, long-time production and complicated procedures (Zaaba et al. 2017). A low cost and simpler GO synthesis approach, which is an electrochemical exfoliation method assisted by surfactant then offers several advantages such as greener, simpler and low-cost production to synthesise GO (Nurhafizah et al. 2015; Parvez et al. 2013; Suriani et al. 2019). Many reports of GO-incorporated membranes for wastewater treatment systems have also successfully increased rejection for different heavy metals (Kochameshki et al. 2017) and dye pollutants (Safarpour et al. 2016; Yang et al. 2017; Zhu et al. 2017). Nonetheless, the agglomeration of GO is the major drawback in the development of GO/PVDF membrane, which can reduce its performance. To prevent GO from agglomeration, the utilisation of surfactant for better dispersion of GO in the polymer matrix is essentially needed.

The previous report showed that the highest CNTs dispersion was achieved by using the triple-tail sodium 1,4-*bis*(neopentyloxy)-3-(neopentyloxycarbonyl)-1,4-dioxobutane-2-silphonate (TC14) surfactant as compared to single- or double-tail surfactant (Mohamed et al. 2014). Suriani et al. (2016) showed that the utilisation of triple-tail TC14 surfactant has presented a smooth surface with low agglomeration of GO when the synthesised GO was intermixed with natural rubber latex. The triple-tail surfactant offers triple interaction during electrochemical exfoliation which resulted in higher dispersion of GO. This result was also in good agreement when the synthesised GO utilising triple-tail TC14 surfactant was used to fabricate thin film

and resulted in higher DSSCs efficiency as compared to the single-tail surfactant (Suriani et al. 2018a, b, c). These confirm that the surfactant's tail number essentially affects the quality of the synthesised GO.

The previous report has also proved that the direct GO synthesis utilising single-tail sodium dodecyl sulphate (SDS) surfactant and DMAc as solvent was successfully achieved and can be used to fabricate NF membrane which resulted in high dye rejection of 92.76% (Suriani et al. 2019). Therefore, it is believed that by using customised double-tail sodium bis(3,5,5-trimethyl-1-hexyl) sulphosuccinate (AOT4) and triple-tail TC14 surfactants, better dispersion and homogeneity of GO-based membrane sheet will be achieved and resulted to better performance for water treatment applications. To the best of our knowledge, the novelty of this study is the utilisation of customised double-tail AOT4 and triple-tail TC14 surfactant for the GO synthesis by electrochemical exfoliation method for dye rejection application. It is believed that the utilisation of both surfactants in the fabrication of the PVDF/GO-based hybrid membrane will increase the hydrophilicity, water flux, dye rejection and anti-fouling performance.

Materials and Methods

Materials

The customised double-tail AOT4 and triple-tail TC14 surfactants (see Table 1), graphite rods (99.99 %, 150 mm in length and 10 mm in diameter, GoodFellow GmbH, Germany) and DMAc were used for GO synthesis. PVDF (Kynar 760, grade in palette form) as a polymer material and titanium (IV) oxide ($\geq$ 99.5%, Sigma-Aldrich) as an additive were used to fabricate the NF membrane. Meanwhile, the MB dye (Sigma-Aldrich) was used for the dye rejection test.
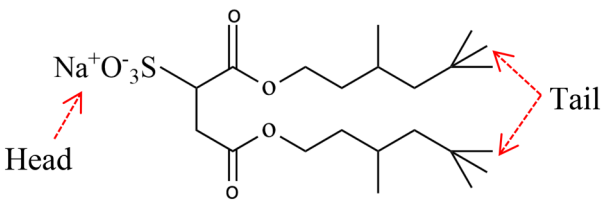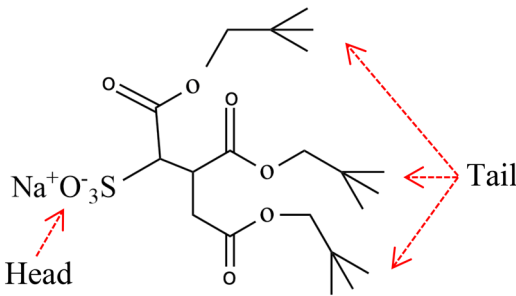
DMAc-Based GO Synthesis

GO was synthesised via electrochemical exfoliation as mentioned in the previous works (Suriani et al. 2018a, b, c) by utilising DMAc as an electrolyte. In brief, AOT4 and TC14 were dissolved in DMAc to form the 0.1 M of the electrolyte, respectively. Then, two graphite rods were partially immersed in the prepared electrolyte and connected to the DC power supply (7 V) for 24 h of GO synthesis time.

Preparation of NF Membranes

The NF membrane was prepared by the non-solvent induced phase separation (NIPS) method. 20 wt% of PVDF and 1 wt% of TiO$_2$ were dissolved to the 79 wt% of the synthesised DMAc_AOT4 and DMAc_TC14 solution, respectively and

Table 1 Surfactant's molecular structure used in this study

Surfactant	Surfactant molecular structure	Chemical name
AOT4		Sodium *bis*(3,5,5-trimethyl-1-hexyl) sulphosuccinate
TC14		Sodium 1,4-*bis*(neopentyloxy)-3-(neopentyloxycarbonyl)-1,4-dioxobutane-2-sulphonate

mechanically stirred at 70 °C for 48 h until a homogeneous solution was obtained. Then, the well-mixed casting solution was kept at room temperature overnight to remove the air bubbles. Next, the fully degassing membrane solution was cast using a casting knife on a clean glass plate with 200 mμ casting gap. Afterward, the casted membrane was directly immersed in deionised (DI) water overnight. The fabricated NF membrane was kept by soaking it in DI water until further characterisation.

Membrane Characterisation

The membrane surface and cross-section morphology were characterised by field emission scanning electron microscopy (Hitachi SU8020). Liquid nitrogen immersion was carried out prior to FESEM observation to crack the membrane samples and further coated with a thin sputtered gold layer. The elemental compositions of the samples were directly confirmed by an EDX instrument (Horiba EMAX). The structural properties of the fabricated NF membranes were studied using micro-Raman spectroscopy (Renishaw InVia microRaman System). Moreover, the hydrophilicity of the fabricated membranes was investigated using contact angle measurement by placing the dry membrane on a glass slide and conducting drop shape analysis (DSA100, KrussGmbH, Germany). The membrane porosity was determined through the gravimetric method by using the following equation:

$$\varepsilon = \frac{(w_1 - w_2)/\rho_w}{[(w_1 - w_2)/\rho_w)] + (w_2/\rho_p)} \times 100\%. \tag{1}$$

where ε is membrane porosity (%), w_1 and w_2 were the wet and dry membrane weights (g), respectively, ρ_w is the water density (0.998 g/cm^3), and ρ_p is the PVDF density (1.78 g/cm^3).

Water flux, dye rejection and antifouling measurement were evaluated using a dead-end stirred membrane evaluation cell system (Sterlitech HP4750) with a capacity of 300 mL and an effective area of 14.6 cm^2. All membrane samples were pressurised with DI water at 0.6 MPa for 30 min before measurement for the compression test. Then, water flux measurement was performed for 10 min measurement with 5 different pressure levels (0.1–0.5 MPa), respectively. The water flux was then estimated using the following equation:

$$J = \frac{V}{A \Delta t}. \tag{2}$$

where J is the permeated flux (L/m^{2}h), V is the permeated water volume (m^3), A is the membrane area (m^2), and Δt is the operating time (h).

Next, the dye rejection test was performed by utilising 10 ppm concentration of MB solution. The absorbance of the treated dye solution was then measured using UV–Vis spectroscopy. The dye rejection efficiency was calculated using the following equation:

$$R(\%) = \left[1 - \frac{C_p}{C_o}\right] \times 100\%. \tag{3}$$

where R is the dye rejection efficiency (%), C_p is the permeate dye concentration (ppm), and C_o is the initial dye concentration (ppm). Subsequently, the antifouling measurement

was done by pressuring the post-treated membrane with DI water for 30 min before performing the water flux measurement at 0.2 MPa for 10 min. The flux recovery ratio (FRR) was calculated by the following formula:

$$\text{FRR} = \left[\frac{J_{w2}}{J_{w1}}\right] \times 100\%. \tag{4}$$

where FRR is the flux recovery ratio, J_{w1} and J_{w2} are water flux before and after measurement, respectively. Operations of some characterisation items can refer to the literatures (Li et al. 2020; Liu et al. 2020; Rao et al. 2020; Xu et al. 2021).

Results and Discussion

Morphological Properties of NF Membranes

FESEM analysis was carried out to investigate the surface and cross-section morphology of the fabricated NF membranes and the results are presented in Fig. 1. Based on Fig. 1a, AOT4-GO clearly spreads all over PVDF/AOT4-GO/TiO$_2$ sample (red arrows) and possess a smooth surface without any crack. This indicated good dispersion of GO in membrane matrix, good stability and durable surface of the fabricated NF membranes (Safarpour et al. 2016; Zinadini et al. 2014). By utilising higher magnification, it was also observed that PVDF/AOT4-GO/TiO$_2$ membrane's surface possessed pores with a diameter range from 27.8–59.5 nm (Fig. 1b). Based on its cross-section view, there are two layers which exhibited a typical asymmetric membrane structure formed for PVDF/AOT4-GO/TiO$_2$. As presented in Fig. 1c, PVDF/AOT4-GO/TiO$_2$ has a thin and dense skin layer which was supported by a macro-voids structure. The bottom sub-layer of this membrane is a sponge-like structure. Further EDX analysis also confirmed the presence of C, O, F, Na, S and Ti as the component of the fabricated NF membranes as depicted in Fig. 1d. PVDF/AOT4-GO/TiO$_2$ contains C and O atomic percentages of 36.95 and 0.97%, respectively. The existence of AOT4 in PVDF/AOT4-GO/TiO$_2$ sample also can be proven by the atomic percentage of Na and S (2.75 and 1.71%, respectively) in the fabricated membrane. Meanwhile, a low Au atomic percentage of around 1.15% was caused by the thin gold coating for FESEM analysis.

Next, Fig. 1e showed that the fabricated PVDF/TC14-GO/TiO$_2$ NF membrane also has a smooth surface without any agglomeration or crack. TC14-GO was also observed to be well-dispersed in the membrane matrix as shown by red arrows. According to Fig. 1f, the larger pore size of PVDF/TC14-GO/TiO$_2$ (27.8–91.3 nm) was clearly seen as compared to PVDF/AOT4-GO/TiO$_2$. This might be attributed to the effect of higher GO content in PVDF/TC14-GO/
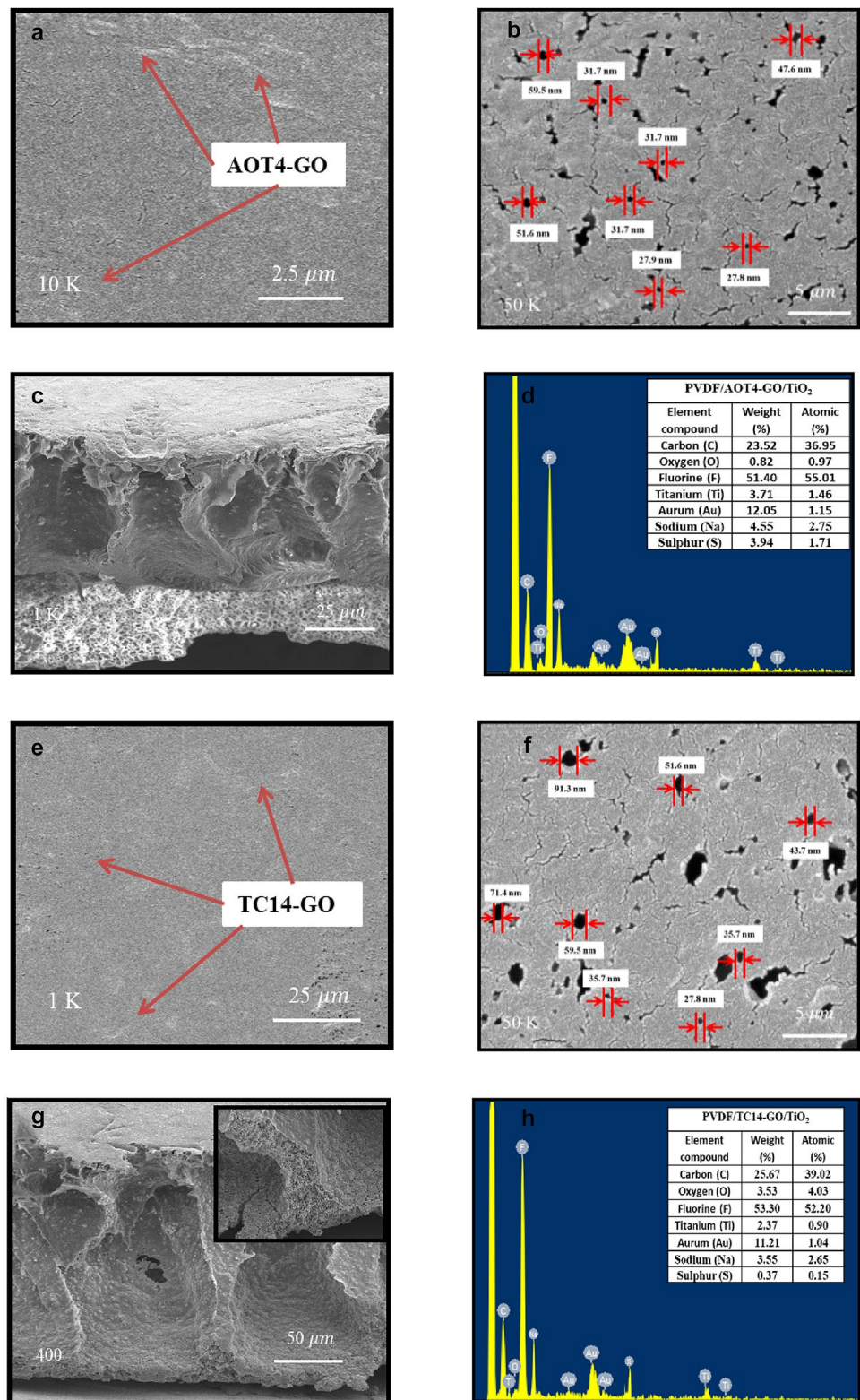
TiO$_2$ resulted from electrochemical exfoliation utilising higher surfactant's tail number. The PVDF/TC14-GO/TiO$_2$ NF membrane displayed a thin and dense skin layer with a well-developed of wider and longer macro-voids structure surrounded by sponge-like layer compared to PVDF/AOT4-GO/TiO$_2$ (Fig. 1g). In contrast with PVDF/AOT4-GO/TiO$_2$, the bottom sub-layer (sponge-like) of PVDF/TC14-GO/TiO$_2$ was almost unobservable (see insert picture) which might be caused by higher GO content in the sample (Zhu et al. 2017). In the previous study, it had been confirmed that the surfactant's tail-number influenced the quality of the synthesised GO (Suriani et al. 2018a). Higher surfactant's tail number in electrochemical exfoliation process was believed to also resulted in a higher amount of GO which noticeably influence the pores structure. The abundance hydrophilic group in GO (oxygen-functional groups) increased the membrane's hydrophilicity thus accelerated the water diffusion during the exchange of non-solvent and solvent and led to the formation of larger macro-voids structure (Méricq et al. 2015; Yang et al. 2017). EDX analysis further confirmed that PVDF/TC14-GO/TiO$_2$ presented a higher C and O atomic percentage (39.02 and 4.03%, respectively) as compared to PVDF/AOT4-GO/TiO$_2$ (Fig. 1h). The presence of Na (3.55%) and S (0.15%) further proved the existence of TC14 surfactant in the PVDF/TC14-GO/TiO$_2$ sample. A low Au atomic percentage of around 1.04% indicated the thin gold coating for FESEM analysis.

Functional Groups of NF Membranes

Raman spectroscopy is a useful technique to confirm the existence of GO in the fabricated membrane. Overall, micro-Raman spectra of both fabricated membranes showed a similar pattern as shown in Fig. 2. There are several peaks correspond to TiO$_2$ and GO in the range of 147.12–1579.80 cm^{-1} which confirmed their existence as additives. However, PVDF peaks were unobservable for both membranes due to their low intensity as stated in the previous study (Suriani et al. 2019). TiO$_2$ peaks were observed at 147.12, 392.73, 510.35 and 635.19 cm^{-1} and also 149.13, 396.69, 512.41, and 638.23 cm^{-1} for PVDF/AOT4-GO/TiO$_2$ and PVDF/TC14-GO/TiO$_2$, respectively. These peaks were corresponding to the E_g, B_{1g}, A_{1g} and E_g modes of the anatase phase of TiO$_2$.

Moreover, micro-Raman spectra of D- and G-band as the characteristic of the carbon material were observed for both fabricated NF membranes. PVDF/AOT4-GO/TiO$_2$ and PVDF/TC14-GO/TiO$_2$ possessed the D- and G-band at 1330.55 and 1579.80 cm^{-1} and also 1331.16 and 1579.37 cm^{-1}, respectively. The D-peak corresponded to the carbon lattice distortion, while G-peak confirmed the sp^2 hybridisation of the carbon atom (Ai et al. 2018). The shifted D- and G-band peak of PVDF/TC14-GO/TiO$_2$

Fig. 1 FESEM images and EDX analysis of the fabricated NF membranes; (**a–d**) PVDF/AOT4-GO/TiO_2 and (**e–h**) PVDF/TC14-GO/TiO_2

PVDF/AOT4-GO/TiO_2		
Element compound	Weight (%)	Atomic (%)
Carbon (C)	23.52	36.95
Oxygen (O)	0.82	0.97
Fluorine (F)	51.40	55.01
Titanium (Ti)	3.71	1.46
Aurum (Au)	12.05	1.15
Sodium (Na)	4.55	2.75
Sulphur (S)	3.94	1.71

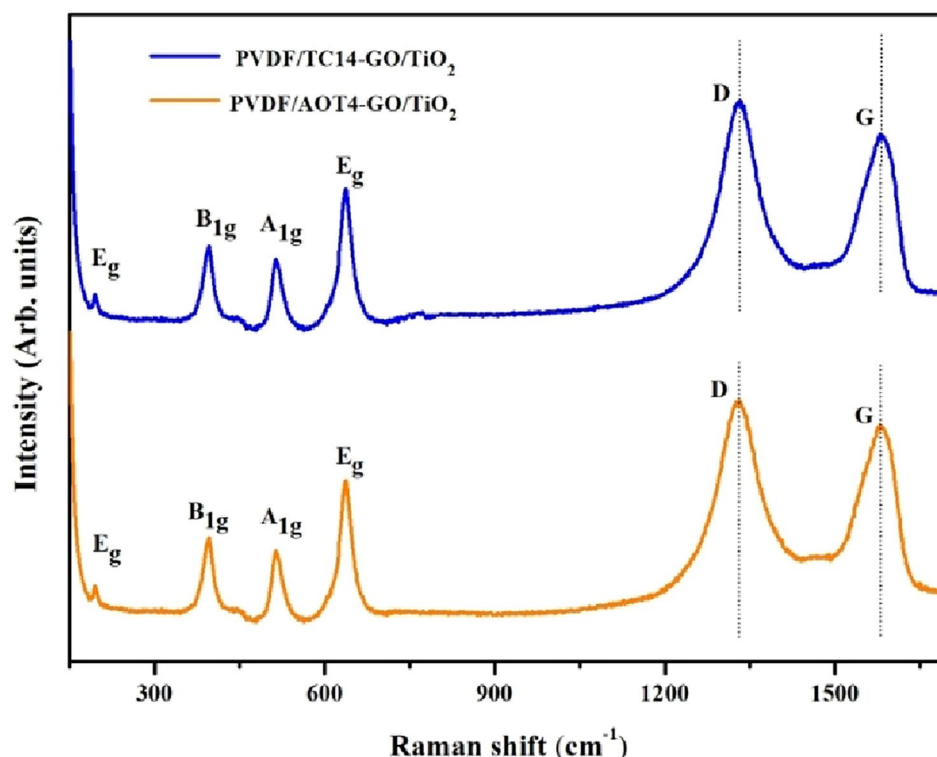| PVDF/TC14-GO/TiO_2		
Element compound	Weight (%)	Atomic (%)
Carbon (C)	25.67	39.02
Oxygen (O)	3.53	4.03
Fluorine (F)	53.30	52.20
Titanium (Ti)	2.37	0.90
Aurum (Au)	11.21	1.04
Sodium (Na)	3.55	2.65
Sulphur (S)	0.37	0.15

compared to PVDF/AOT4-GO/TiO_2 was might be due to a higher oxidation process during electrochemical exfoliation resulted from higher surfactants' tail number. This was also confirmed by higher D-band peak intensity (I_D) of PVDF/TC14-GO/TiO_2 compared to PVDF/AOT4-GO/TiO_2 which indicated a higher defect level (Khan et al. 2010). In addition, lower G-band peak intensity (I_G) of

Fig. 2 Micro-Raman spectra of the fabricated PVDF/AOT4-GO/TiO$_2$ and PVDF/TC14-GO/TiO$_2$ NF membrane


PVDF/TC14-GO/TiO$_2$ indicated a decreased number of exfoliated GO layer (Díez-Pascual et al. 2018).

I_D/I_G ratio can be used to investigate the defect level of the sample. Based on the calculation, PVDF/TC14-GO/TiO$_2$ presented a higher defect level of the synthesised GO which indicated by a higher I_D/I_G ratio (1.13) compared to PVDF/AOT4-GO/TiO$_2$ (1.06) (Francolini et al. 2019; Kaniyoor and Ramaprabhu 2012; Khan et al. 2010). In addition, it also showed higher oxygen-functional groups of PVDF/TC14-GO/TiO$_2$ resulted from electrochemical exfoliation than PVDF/AOT4-GO/TiO$_2$ (Francolini et al. 2019; Luo et al. 2018; Yu et al. 2015). This result further confirmed that the utilisation of triple-tail TC14 surfactant leads to higher interaction during GO synthesis thus resulted in better GO dispersion.

Hydrophilicity, Contact Angle and Porosity Properties of NF Membrane

Contact angle measurement was then used to investigate the membrane's surface hydrophilicity. From literature, pure PVDF have the highest contact angle (77.1°–104.3°) as compared to the hybrid membrane (Nikooe and Saljoughi 2017; Nor et al. 2016; Zhang et al. 2012; Zheng et al. 2016). It is well established that utilising the additive has an influence on the contact angle measurement. In comparison with pure PVDF in the previous study, both of the membranes presented smaller contact angle. However, as depicted in Fig. 3, PVDF/AOT4-GO/TiO$_2$ presented a higher contact angle value of 75.2 ± 0.24° (Fig. 3a) as compared to PVDF/TC14-GO/TiO$_2$ [65.4 ± 0.17° (Fig. 3b)]. This indicated that membrane's hydrophilicity improved as the amount of GO

Fig. 3 Contact angle measurement of the fabricated; (**a**) PVDF/AOT4-GO/TiO$_2$ and (**b**) PVDF/TC14-GO/TiO$_2$ NF membrane
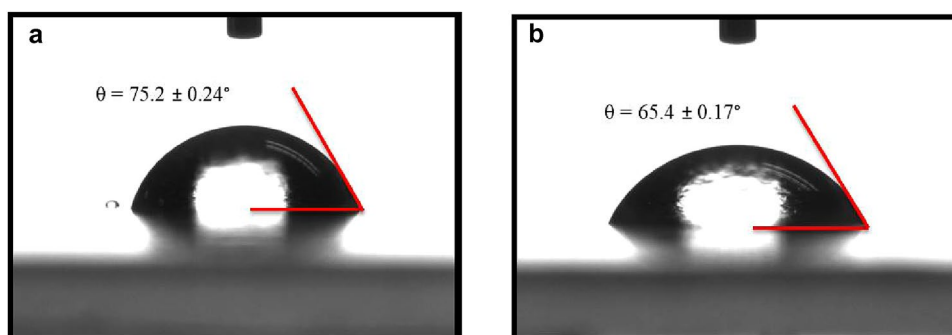
content in the PVDF/TC14-GO/TiO$_2$ membrane increased. This was believed due to the utilisation of triple-tail TC14 which provides an extra chain for GO and PVDF polymer interconnection (Lai et al. 2019). In addition, the abundance number of oxygen-containing functional groups of GO resulted in higher water molecule diffusion rate through the membrane caused by the hydrogen bond (Ai et al. 2018). As a result, the membrane becomes more hydrophilic and own a lower contact angle.

Further porosity measurement revealed that PVDF/TC14-GO/TiO$_2$ presented higher porosity (83.31%) as compared to PVDF/AOT4-GO/TiO$_2$ (79.35%). This result was in good agreement with FESEM images of PVDF/TC14-GO/TiO$_2$ (Fig. 1f) which shows a bigger pore size than PVDF/AOT4-GO/TiO$_2$ (Fig. 1b). Triple-tail TC14 surfactant plays a crucial role during the GO synthesis as a higher exfoliated GO amount was obtained compared to the double-tail AOT4 surfactant. Higher GO amount in PVDF/TC14-GO/TiO$_2$ sample leads to higher porosity and bigger pore size which increased the mass transfer rate between the solvent and the non-solvent during phase inversion (Zhu et al. 2017; Zinadini et al.

2014). In addition, higher porosity of the PVDF/TC14-GO/TiO$_2$ was might be caused by lower casting solution viscosity during the phase inversion process which then resulted in instantaneous demixing process (Ai et al. 2018). The contact angle and porosity value of the fabricated membranes are summarised in Table 2.

Water Flux of Fabricated Membranes Based on Different Operating Pressures

Pure water flux was measured to study the permeability of the prepared membranes. As presented in Fig. 4, water flux increased significantly with the increment of the operating pressure. As shown in Table 3, PVDF/TC14-GO/TiO$_2$ water permeability was observed to be three times higher (48.968 L/m^2 h MPa) as compared to PVDF/AOT4-GO/TiO$_2$ (16.533 L/m^2 h MPa) which was believed affected by its higher hydrophilicity and porosity. In addition, it also confirmed that higher water permeability of the fabricated NF membrane was achieved as GO content

Table 2 Contact angle and porosity values of the fabricated NF membranes

Membrane	Contact angle (°)	Porosity (%)
PVDF/AOT4-GO/TiO$_2$	75.2±0.24	79.35
PVDF/TC14-GO/TiO$_2$	65.4±0.17	83.31

Table 3 Water permeability of the fabricated PVDF/AOT4-GO/TiO$_2$ and PVDF/TC14-GO/TiO$_2$ NF membranes

Membrane	Water permeability (L/m^2 h MPa)
PVDF/AOT4-GO/TiO$_2$	16.533
PVDF/TC14-GO/TiO$_2$	48.968

Fig. 4 Water flux measurements of the fabricated NF membranes based on different driving pressure level
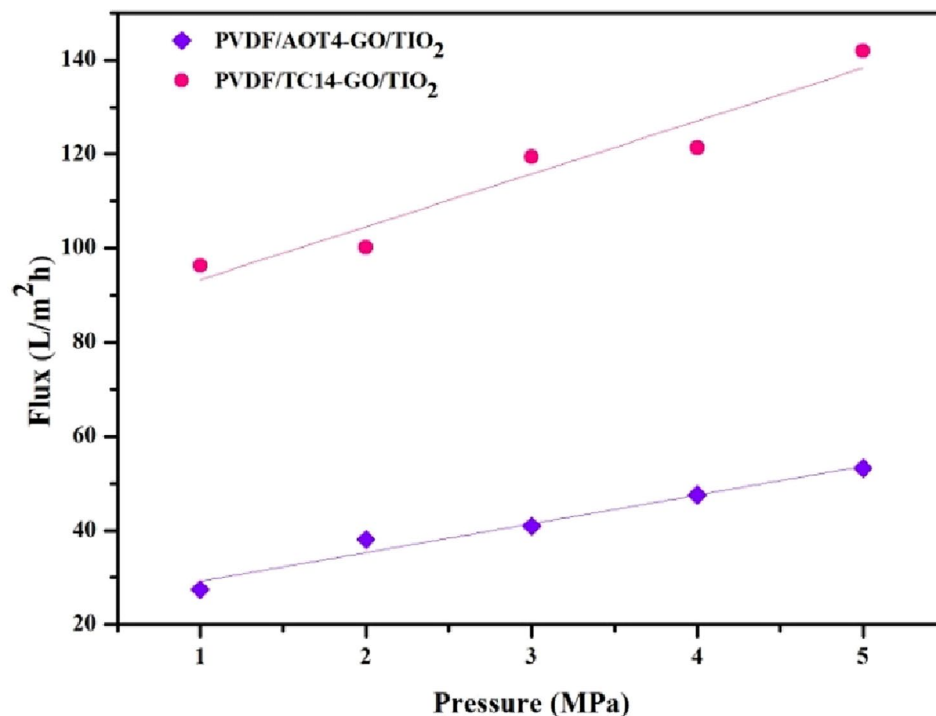
increased. The utilisation of triple-tail TC14 surfactant was believed resulted in higher exfoliated GO content as well as hydrophilic functional groups (PVDF/TC14-GO/TiO$_2$ sample) as compared to double-tail AOT4 surfactant (PVDF/TC14-GO/TiO$_2$ sample). This was also supported by the large macro-voids structure of PVDF/TC14-GO/TiO$_2$ (see FESEM images) which attracted and promoted the water molecules to pass through the membrane (Ai et al. 2018; Wang et al. 2018; Xia and Ni 2014). These results were also supported by membrane's pore sizes and pure water flux for both membranes.

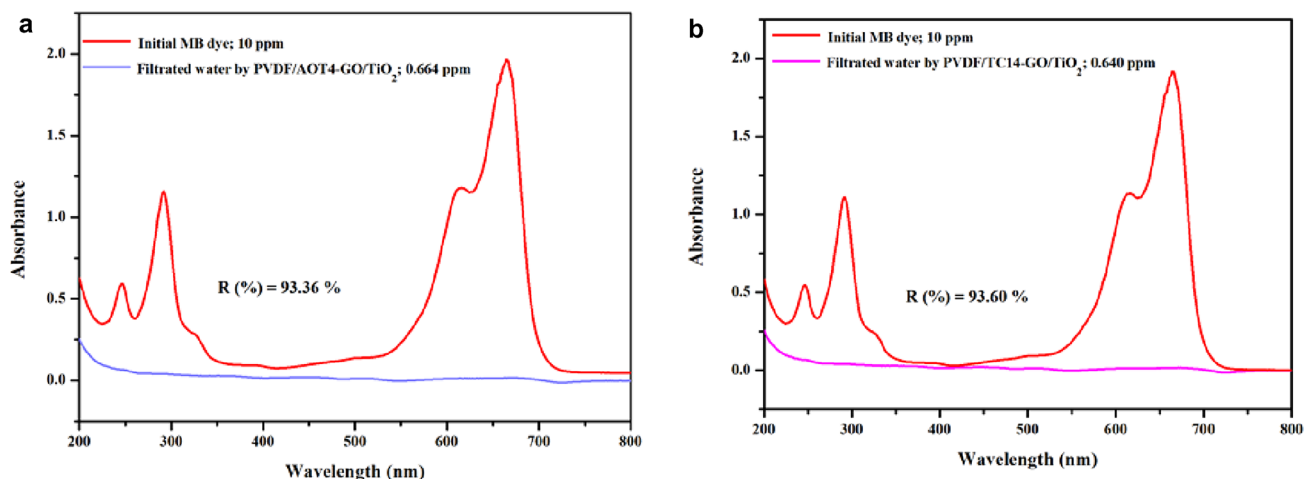## Dye Rejection Performance of the Fabricated NF Membranes

Based on dead-end cell measurement, PVDF/TC14-GO/TiO$_2$ showed slightly higher dye rejection efficiency (*R*) value (92.61%) as compared to PVDF/AOT4-GO/TiO$_2$ membrane (92.39%) as shown in Fig. 5. However, PVDF/TC14-GO/TiO$_2$ possessed three times higher dye flux (91.106 L/m^2 h) as compared to PVDF/AOT4-GO/TiO$_2$ (34.384 L/m^2 h) (see Table 4). These results further confirmed that embedding triple-tail TC14-GO into the casting solution has improved the dye rejection as well as high permeability in comparison with double-tail AOT4-GO. This was believed related to the extra chain interconnection between GO and PVDF provided by triple-tail TC14 surfactant which resulted higher GO content in the PVDF/TC14-GO/TiO$_2$ thus improved the hydrophilicity and porosity value. These results lead to the conclusion that the utilisation of a higher surfactant's tail number in the GO synthesis process affected the dye flux and dye rejection efficiency.

Table 4 Dye rejection performance of the fabricated nf membranes measured at a pressure of 2 MPa

| Membrane	Dye flux (L/m^2 h)	Final concentration (ppm)	Rejection rate (%)
PVDF/AOT4-GO/TiO$_2$	34.384	0.760	92.39
PVDF/TC14-GO/TiO$_2$	91.106	0.738	92.61

Antifouling Properties of the Fabricated NF Membranes

Assessment of the fabricated NF membranes on long-term performance has been evaluated by their fouling. Filtration activity has caused the dye's organic molecules deposited on the membrane surface then permeate into the membrane which then contributed to the membrane fouling (Nikooe and Saljoughi 2017). Antifouling characteristics of the prepared membranes were then studied through the FRR. Based on Fig. 6, the flux decline curve of PVDF/TC14-GO/TiO$_2$ decayed rapidly during the first 3 min before being stabilised gradually. Meanwhile, slower flux decline was observed for PVDF/AOT4-GO/TiO$_2$ which indicated better antifouling properties (Zhu et al. 2017). In general, lower organic adsorption at the membrane surface makes it easier to be cleaned (Zhang et al. 2013). Before the membrane was cleaned, the pure water flux of PVDF/AOT4-GO/TiO$_2$ and PVDF/TC14-GO/TiO$_2$ at the same pressure was 38.082 and 100.137 L/m^2 h, respectively. However, after the membrane was cleaned, the FRR for PVDF/AOT4-GO/TiO$_2$ was higher (166%) than PVDF/TC14-GO/TiO$_2$ (119%), indicated an excellent organic molecules adsorption resistance (Wang et al. 2015). This result confirmed that the different GO content in both membranes clearly affects the FRR value. The

Fig. 5 Dye rejection measurement of the fabricated NF membrane by using UV–Vis spectroscopy; (**a**) PVDF/AOT4-GO/TiO$_2$ and (**b**) PVDF/TC14-GO/TiO$_2$

Fig. 6 Flux decline curve of the fabricated NF membranes measured at 2 MPa pressure
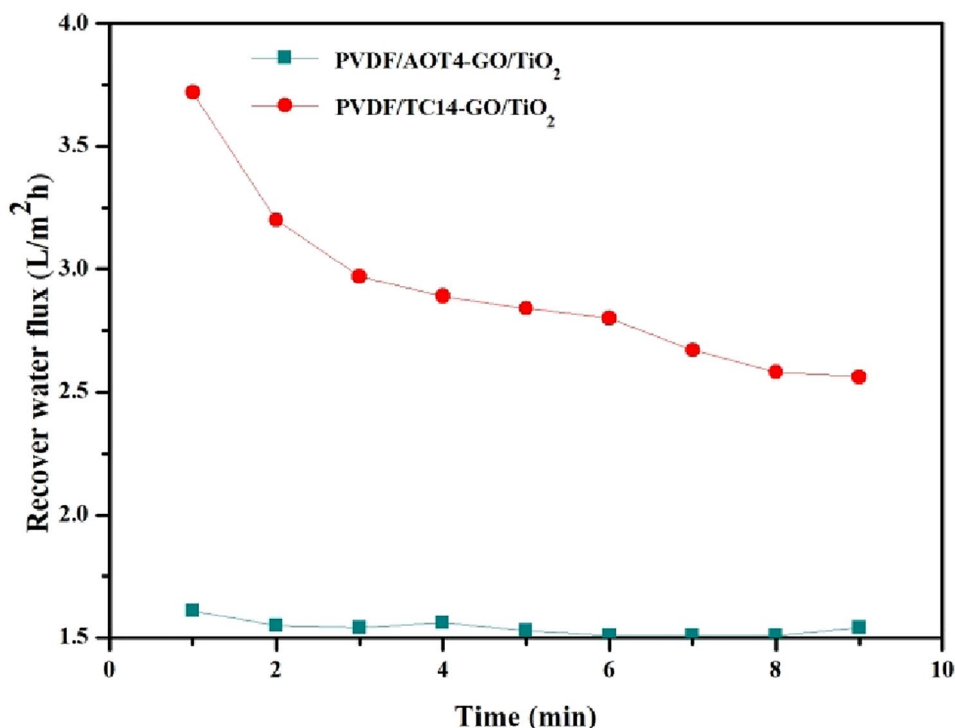
lower FRR value presented by PVDF/TC14-GO/TiO$_2$ was believed due to its large pores size which leading to some fouling blocked and adsorbed onto the membrane surface. Therefore, the volume available for passage of the permeate were then reduced (Coutinho et al. 2009).

Conclusions

In this work, PVDF/AOT4-GO/TiO$_2$ and PVDF/TC14 -GO/TiO$_2$ NF membranes were successfully fabricated via NIPS method utilising customised double-tail AOT4 and triple-tail TC14 surfactants for GO synthesis via electrochemical exfoliation. Based on several measurements, it was found that the utilisation of a higher surfactant's tail number resulted in larger macro-voids structure with higher membrane's porosity and pore size. In addition, higher membrane hydrophilicity was also achieved as the contact angle decreased. PVDF/TC14-GO/TiO$_2$ presented three times higher water permeability (48.968 L/m^2 h MPa) and dye flux (91.106 L/m^2 h). Moreover, its FRR high value (119%) indicated good antifouling performance. The obtained results suggest that the addition of TiO$_2$ and different type of GO as additives play an important role to enhance the dye rejection and antifouling performance.

References

Ai J, Yang L, Liao G, Xia H, Xiao F (2018) Applications of graphene oxide blended poly(vinylidene fluoride) membranes for the treatment of organic matters and its membrane fouling investigation. Appl Surf Sci 455:1–40. https://doi.org/10.1016/j.apsusc.2018.05.162

Aid S, Eddhahak A, Khelladi S, Ortega Z, Chaabani S, Tcharkhtchi A (2019) On the miscibility of PVDF/PMMA polymer blends: thermodynamics, experimental and numerical investigations. Polym Testing 73:222–231. https://doi.org/10.1016/j.polymertesting.2018.11.036

Anvari A, Yancheshme AA, Rekaabdar F, Hemmati M, Tavakolmoghadam M, Safekordi A (2017) PVDF/PAN blend membrane: preparation, characterization and fouling analysis. J Polym Environ 25(4):1348–1358. https://doi.org/10.1007/s10924-016-0889-x

Contreras MM, Nascimento CR, Cucinelli Neto RP, Teixeira S, Berry N, Costa MF, Costa CA (2018) TD-NMR analysis of structural evolution in PVDF induced by stress relaxation. Polym Testing 68:153–159. https://doi.org/10.1016/j.polymertesting.2018.03.051

de Coutinho CM, Chiu MC, Basso RC, Ribeiro APB, Gonçalves LAG, Viotto LA (2009) State of art of the application of membrane technology to vegetable oils: a review. Food Res Intern 42:536–550. https://doi.org/10.1016/j.foodres.2009.02.010

Díez-Pascual A, Vallés C, Mateos R, Vera-López S, Kinloch IA, Andrésa MPS (2018). Influence of surfactants of different nature and chain length on the morphology, thermal stability and sheet resistance of graphene. Soft Matter 1–36. https://doi.org/10.1039/C8SM01017J

Escobar IC, Van Der Bruggen B (2015) Microfiltration and ultrafiltration membrane science and technology. J Appl Polym Sci 132(21). https://doi.org/10.1002/app.42002

Francolini I, Perugini E, Silvestro I, Lopreiato M, D'Abusco AS, Valentini F, Placidi E, Arciprete F, Martinelli A, Piozzi A (2019) Graphene oxide oxygen content affects physical and biological

properties of scaffolds based on chitosan/graphene oxide conjugates. Materials 12(7):1142–1158. https://doi.org/10.3390/ma12071142

Freire E, Bianchi O, Martins JN, Monteiro EEC, Forte MMC (2012) Non-isothermal crystallization of PVDF/PMMA blends processed in low and high shear mixers. J Non-Cryst Solids 358(18–19):2674–2681. https://doi.org/10.1016/j.jnoncrysol.2012.06.021

GarcíaDoménech N, Purcell-Milton F, Gunko YK (2020) Recent progress and future prospects in development of advanced materials for nanofiltration. Mat Today Commun 23:100888. https://doi.org/10.1016/j.mtcomm.2019.100888

Guo-dong K, Yi-ming C (2014) Application and modification of poly(vinylidene fluoride) (PVDF) membranes—a review. J Membr Sci 463:145–165. https://doi.org/10.1016/j.memsci.2014.03.055

Huang X, Qi X, Boey F, Zhang H (2012) Graphene-based composites. Chem Soc Rev 41(2):666–686. https://doi.org/10.1039/c1cs15078b

Kaniyoor A, Ramaprabhu S (2012) A Raman spectroscopic investigation of graphite oxide derived graphene. AIP Adv 2(3):1–16. https://doi.org/10.1063/1.4756995

Khan U, O'Neill A, Lotya M, De S, Coleman JN (2010) High-concentration solvent exfoliation of graphene. Small 6(7):864–871. https://doi.org/10.1002/smll.200902066

Kochameshki MG, Marjani A, Mahmoudian M, Farhadi K (2017) Grafting of diallyldimethylammonium chloride on graphene oxide by RAFT polymerization for modification of nanocomposite polysulfone membranes using in water treatment. Chem Eng J 309(October):206–221. https://doi.org/10.1016/j.cej.2016.10.008

Ladewig B, Al-Shaeli MNZ (2017) Fundamentals of membrane bioreactors. Springer Trans Civil Environ Eng 13–38. https://doi.org/10.1007/978-981-10-2014-8

Lai Y, Wan L, Wang B (2019) PVDF/graphene composite nanoporous membranes for vanadium flow batteries. Membranes 9(7):89–101. https://doi.org/10.3390/membranes9070089

Lee C, Wei X, Kysar JW, Hone J (2008) Measurement of the elastic properties and intrinsic strength of monolayer graphene. Science 321(5887):385–388. https://doi.org/10.1126/science.1157996

Li J, Yan B, Shao X, Wang S, Tian H, Zhang Q (2015) Influence of Ag/TiO$_2$ nanoparticle on the surface hydrophilicity and visible-light response activity of polyvinylidene fluoride membrane. Appl Surf Sci 324:82–89. https://doi.org/10.1016/j.apsusc.2014.10.080

Li R, Fan H, Shen L, Rao L, Tang J, Hu S, Lin H (2020) Inkjet printing assisted fabrication of polyphenol-based coating membranes for oil/water separation. Chemosphere 250:126236. https://doi.org/10.1016/j.chemosphere.2020.126236

Liao Y, Loh CH, Tian M, Wang R, Fane AG (2018) Progress in electrospun polymeric nanofibrous membranes for water treatment: fabrication, modification and applications. Prog Polym Sci 77:69–94. https://doi.org/10.1016/j.progpolymsci.2017.10.003

Liu T, Yang B, Graham N, Yu W, Sun K (2017) Trivalent metal cation cross-linked graphene oxide membranes for NOM removal in water treatment. J Membr Sci 542:31–40. https://doi.org/10.1016/j.memsci.2017.07.061

Liu Q, Huang S, Zhang Y, Zhao S (2018) Comparing the antifouling effects of activated carbon and TiO$_2$ in ultrafiltration membrane development. J Colloid Interface Sci 515:109–118. https://doi.org/10.1016/j.jcis.2018.01.026

Liu H, Chen Y, Zhang K, Wang C, Hu X, Cheng B, Zhang Y (2019) Poly(vinylidene fluoride) hollow fiber membrane for high-efficiency separation of dyes-salts. J Membr Sci 578:43–52. https://doi.org/10.1016/J.MEMSCI.2019.02.029

Liu Y, Shen L, Lin H, Yu W, Xu Y, Li R, Sun T, He Y (2020) A novel strategy based on magnetic field assisted preparation of magnetic and photocatalytic membranes with improved performance. J Membr Sci 612:118378. https://doi.org/10.1016/j.memsci.2020.118378

Luo L, Peng T, Yuan M, Sun H, Dai S, Wang L (2018) Preparation of graphite oxide containing different oxygen-containing functional groups and the study of ammonia gas sensitivity. Sensors (Switzerland) 18(11):3745–3759. https://doi.org/10.3390/s18113745

Méricq J, Mendret J, Brosillon S, Faur C (2015) High performance PVDF-TiO$_2$ membranes for water treatment. Chem Eng Sci 123:283–291. https://doi.org/10.1016/j.ces.2014.10.047

Miao W, Li ZK, Yan X, Guo YJ, Lang WZ (2017) Improved ultrafiltration performance and chlorine resistance of PVDF hollow fiber membranes via doping with sulfonated graphene oxide. Chem Eng J 317:901–912. https://doi.org/10.1016/j.cej.2017.02.121

Mohamed A, Anas AK, Abu Bakar S, Aziz AA, Sagisaka M, Brown P et al (2014) Preparation of multiwall carbon nanotubes (MWCNTs) stabilised by highly branched hydrocarbon surfactants and dispersed in natural rubber latex nanocomposites. Colloid Polym Sci 292(11):3013–3023. https://doi.org/10.1007/s00396-014-3354-1

Nikooe N, Saljoughi E (2017) Preparation and characterization of novel PVDF nanofiltration membranes with hydrophilic property for filtration of dye aqueous solution. Appl Surf Sci 413:41–49. https://doi.org/10.1016/j.apsusc.2017.04.029

Nor NAM, Jaafar J, Ismail AF, Mohamed MA, Rahman MA, Othman MHD, Yusof N (2016) Preparation and performance of PVDF-based nanocomposite membrane consisting of TiO$_2$ nanofibers for organic pollutant decomposition in wastewater under UV irradiation. Desalination 391:89–97. https://doi.org/10.1016/j.desal.2016.01.015

Nurhafizah MD, Suriani AB, Suhufa A, Mohamed A, Isa IM, Azlan K, Mohamad RM (2015) The synthesis of graphene oxide via electrochemical exfoliation method. Adv Mater Res 1109(December):55–59. https://doi.org/10.4028/www.scientific.net/AMR.1109.55

Park SJ, Cheedrala RK, Diallo MS, Kim C, Kim IS, Goddard WA (2012) Nanofiltration membranes based on polyvinylidene fluoride nanofibrous scaffolds and crosslinked polyethyleneimine networks. Nanotechnol Sustain Dev First Edn 14(884):33–46. https://doi.org/10.1007/978-3-319-05041-6_3

Park HJ, Bhatti UH, Nam SC, Yeol SP, Lee KB, Hyun BI (2018) Nafion/TiO$_2$ nanoparticle decorated thin film composite hollow fiber membrane for efficient removal of SO$_2$ gas. Sep Purif Technol 211:1–49. https://doi.org/10.1016/j.seppur.2018.10.010

Parvez K, Li R, Puniredd SR, Hernandez Y (2013) Electrochemically exfoliated graphene as solution-processable, highly conductive electrodes for organic electronics. ACS Nano 7(4):3598–3606. https://doi.org/10.1021/nn400576v

Rao L, Tang J, Hu S, Shen L, Xu Y, Li R, Lin H (2020) Inkjet printing assisted electroless Ni plating to fabricate nickel coated polypropylene membrane with improved performance. J Colloid Interface Sci 565:546–554. https://doi.org/10.1016/j.jcis.2020.01.069

Safarpour M, Vatanpour V, Khataee A (2016) Preparation and characterization of graphene oxide/TiO$_2$ blended PES nanofiltration membrane with improved antifouling and separation performance. Desalination 393:65–78. https://doi.org/10.1016/j.desal.2015.07.003

Sangermano M, Farrukh MM, Tiraferri A, Dizman C, Yagci Y (2015) Synthesis, preparation and characterization of UV-cured methacrylated polysulfone-based membranes. Mater Today Commun 5:64–69. https://doi.org/10.1016/j.mtcomm.2015.10.002

Santhosh C, Velmurugan V, Jacob G, Jeong SK, Grace AN, Bhatnagar A (2016) Role of nanomaterials in water treatment applications: a review. Chem Eng J 306:1116–1137. https://doi.org/10.1016/j.cej.2016.08.053

Shon HK, Phuntsho S, Chaudhary DS, Vigneswaran S, Cho J (2013) Nanofiltration for water and wastewater treatment—a mini review. Water Eng Sci 6(1):47–53. https://doi.org/10.5194/dwes-6-47-2013

Sivakumaran R, Kundu S, Kumaran KT, Mishra S, Pandian SP (2016) Synthesis of PVDF/CNT and their functionalized composites for studying their electrical properties to analyze their applicability in actuation & sensing. Colloids Surf A 509:1–20. https://doi.org/10.1016/j.colsurfa.2016.09.007

Suriani AB, Nurhafizah MD, Mohamed A, Masrom AK, Sahajwalla V, Joshi RK (2016) Highly conductive electrodes of graphene oxide/natural rubber latex-based electrodes by using a hyper-branched surfactant. Mater Des 99:174–181. https://doi.org/10.1016/j.matdes.2016.03.067

Suriani AB, Mohamed FA, Hashim MN, Rosmi MS, Abdul Khalil HPS (2018a) Reduced graphene oxide/platinum hybrid counter electrode assisted by custom-made triple-tail surfactant and zinc oxide/titanium dioxide bilayer nanocomposite photoanode for enhancement of DSSCs photovoltaic performance. Optik 161:70–83. https://doi.org/10.1016/j.ijleo.2018.02.013

Suriani AB, Mohamed MA, Mamat MH, Hashim N, Isa IM, Ahmad MK (2018b) Improving the photovoltaic performance of DSSCs using a combination of mixed-phase TiO_2 nanostructure photoanode and agglomerated free reduced graphene oxide counter electrode assisted with hyperbranched surfactant. Optik 158:522–534. https://doi.org/10.1016/j.ijleo.2017.12.149

Suriani AB, Mohamed MA, Othman MHD, Mamat MH, Hashim N, Khalil HPSA (2018c) Reduced graphene oxide-multiwalled carbon nanotubes hybrid film with low Pt loading as counter electrode for improved photovoltaic performance of dye-sensitised solar cells. J Mater Sci Mater Electron 29:10723–10743. https://doi.org/10.1007/s10854-018-9139-4

Suriani AB, Mohamed MA, Othman MHD, Rohani R, Yusoff II, AbdulKhalil HPS (2019) Incorporation of electrochemically exfoliated graphene oxide and TiO_2 into polyvinylidene fluoride-based nanofiltration membrane for dye rejection. Water Air Soil Pollut. https://doi.org/10.1007/s11270-019-4222-x

Teng J, Wu M, Chen J, Lin H, He Y (2020) Different fouling propensities of loosely and tightly bound extracellular polymeric substances (EPSs) and the related fouling mechanisms in a membrane bioreactor. Chemosphere 255:126953. https://doi.org/10.1016/j.chemosphere.2020.126953

Van Tran TT, Kumar SR, Lue SJ (2019) Separation mechanisms of binary dye mixtures using a PVDF ultrafiltration membrane: Donnan effect and intermolecular interaction. J Membr Sci 575:38–49. https://doi.org/10.1016/j.memsci.2018.12.070

Vo LT, Giannelis EP (2007) Compatibilizing poly(vinylidene fluoride)/nylon-6 blends with nanoclay. Macromolecules 40(23):8271–8276. https://doi.org/10.1021/ma071508q

Wang J, Lang WZ, Xu HP, Zhang X, Guo YJ (2015) Improved poly(vinyl butyral) hollow fiber membranes by embedding multiwalled carbon nanotube for the ultrafiltrations of bovine serum albumin and humic acid. Chem Eng J 260:90–98. https://doi.org/10.1016/j.cej.2014.08.082

Wang J, Wang Y, Zhu J, Zhang Y, Liu J, Van der Bruggen B (2017) Construction of TiO_2@graphene oxide incorporated antifouling nanofiltration membrane with elevated filtration performance. J Membr Sci 533:279–288. https://doi.org/10.1016/j.memsci.2017.03.040

Wang F, Wu Y, Huang Y (2018) Novel application of graphene oxide to improve hydrophilicity and mechanical strength of aramid nanofiber hybrid membrane. Compos A Appl Sci Manuf 110:126–132. https://doi.org/10.1016/j.compositesa.2018.04.023

Wu L, Zhang X, Wang T, Du C, Yang C (2018) Enhanced performance of polyvinylidene fluoride ultrafiltration membranes by incorporating TiO_2/graphene oxide. Chem Eng Res Des 141:492–501. https://doi.org/10.1016/j.cherd.2018.11.025

Wu M, Chen Y, Lin H, Zhao L, Shen L, Li R, Xu Y, Hong H, He Y (2020) Membrane fouling caused by biological foams in a submerged membrane bioreactor: mechanism insights. Water Res 181:115932. https://doi.org/10.1016/j.watres.2020.115932

Xia S, Ni M (2014) Preparation of poly(vinylidene fluoride) membranes with graphene oxide addition for natural organic matter removal. J Membr Sci 473:54–62. https://doi.org/10.1016/j.memsci.2014.09.018

Xu Y, Xiao Y, Zhang W, Lin H, Shen L, Li R (2021) Plant polyphenol intermediated metal-organic framework (MOF) membranes for efficient desalination. J Membr Sci 618:118726. https://doi.org/10.1016/j.memsci.2020.118726

Yang M, Zhao C, Zhang S, Li P, Hou D (2017) Preparation of graphene oxide modified poly(m-phenylene isophthalamide) nanofiltration membrane with improved water flux and antifouling property. Appl Surf Sci 394:149–159. https://doi.org/10.1016/j.apsusc.2016.10.069

Yao YW, Cui LH, Li Y, Yu NC, Dong HS, Chen X, Wei F (2015) Electrocatalytic degradation of methyl orange on PbO_2–TiO_2 nanocomposite electrodes. Intern J Environ Res 9(4):1357–1364. https://doi.org/10.22059/ijer.2015.1028

Yu P, Lowe SE, Simon GP, Zhong YL (2015) Electrochemical exfoliation of graphite and production of functional graphene. Curr Opin Colloid Interface Sci 20:329–338. https://doi.org/10.1016/j.cocis.2015.10.007

Zaaba NI, Foo KL, Hashim U, Tan SJ, Liu WW, Voon CH (2017) Synthesis of graphene oxide using modified hummers method: solvent influence. Procedia Eng 184:469–477. https://doi.org/10.1016/j.proeng.2017.04.118

Zhang X, Wang Y, You Y, Meng H, Zhang J, Xu X (2012) Preparation, performance and adsorption activity of TiO_2 nanoparticles entrapped PVDF hybrid membranes. Appl Surf Sci 263:660–665. https://doi.org/10.1016/j.apsusc.2012.09.131

Zhang J, Xu Z, Shan M, Zhou B, Li Y, Li B, Qian X (2013) Synergetic effects of oxidized carbon nanotubes and graphene oxide on fouling control and anti-fouling mechanism of polyvinylidene fluoride ultrafiltration membranes. J Membr Sci 448:81–92. https://doi.org/10.1080/10584587.2013.787842

Zhang R, Liu Y, He M, Su Y, Elimelech M, Zhongyi J (2016) Antifouling membranes for sustainable water purification: strategies and mechanisms. Chem Soc Rev 45:5888–5924. https://doi.org/10.1039/C5CS00579E

Zhang J, Wang Z, Wang Q, Pan C, Wu Z (2017) Comparison of antifouling behaviours of modified PVDF membranes by TiO_2 sols with different nanoparticle size: implications of casting solution stability. J Membr Sci 525:378–386. https://doi.org/10.1016/j.memsci.2016.12.021

Zheng W, Yu S, Jiang Q, Zhao Z, Yu W, Zhang Y (2009) Formation mechanism of β-phase in PVDF/CNT composite prepared by the sonication method. Macromolecules 42(22):8870–8874. https://doi.org/10.1021/ma901765j

Zheng G, He Y, Yu Z, Zhan Y, Ma L, Zhang L (2016) Preparation and characterization of a novel PVDF ultrafiltration membrane by blending with TiO_2-HNTs nanocomposites. Appl Surf Sci. https://doi.org/10.1016/j.apsusc.2016.02.211

Zhu Z, Wang L, Xu Y, Li Q, Jiang J, Wang X (2017) Preparation and characteristics of graphene oxide-blending PVDF nanohybrid membranes and their applications for hazardous dye adsorption and rejection. J Colloid Interface Sci 504:429–439. https://doi.org/10.1016/j.jcis.2017.05.068

Zinadini S, Zinatizadeh AA, Rahimi M, Vatanpour V, Zangeneh H (2014) Preparation of a novel antifouling mixed matrix PES membrane by embedding graphene oxide nanoplates. J Membr Sci 453:292–301. https://doi.org/10.1016/j.memsci.2013.10.070

Affiliations

R. Mohamat[1,2] · A. B. Suriani[1,2] 🔵 · A. Mohamed[1,3] · Muqoyyanah[1,2] · M. H. D. Othman[4] · R. Rohani[5] · M. H. Mamat[6] · M. K. Ahmad[7] · M. N. Azlan[2] · M. A. Mohamed[8] · M. D. Birowosuto[9] · T. Soga[10]

1. Nanotechnology Research Centre, Faculty of Science and Mathematics, Universiti Pendidikan Sultan Idris, Tanjung Malim, 35900 Perak, Malaysia

2. Department of Physics, Faculty of Science and Mathematics, Universiti Pendidikan Sultan Idris, Tanjung Malim, 35900 Perak, Malaysia

3. Department of Chemistry, Faculty of Science and Mathematics, Universiti Pendidikan Sultan Idris, Tanjung Malim, 35900 Perak, Malaysia

4. Advanced Membrane Technology Research Centre (AMTEC), Universiti Teknologi Malaysia, 81310 Skudai, Johor, Malaysia

5. Department of Chemical and Process Engineering, Faculty of Engineering and Built Environment, Universiti Kebangsaan Malaysia, UKM, 43600 Bangi, Selangor, Malaysia

6. NANO-ElecTronic Centre (NET), Faculty of Electrical Engineering, Universiti Teknologi MARA (UiTM), 40450 Shah Alam, Selangor, Malaysia

7. Microelectronic and Nanotechnology-Shamsuddin Research Centre (MiNT-SRC), Faculty of Electrical and Electronic Engineering, Universiti Tun Hussein Onn Malaysia, Parit Raja, Malaysia

8. Institute of Microengineering and Nanoelectronics (IMEN), Universiti Kebangsaan Malaysia, UKM, 43600 Bangi, Selangor, Malaysia

9. CNRS International NTU Thales Research Alliance (CINTRA), Research Techno Plaza, 50 Nanyang Drive, Border X Block, Singapore 637553, Singapore

10. Department of Frontier Materials, Nagoya Institute of Technology, Gokiso-cho, Showa-ku, Nagoya 466-8555, Japan